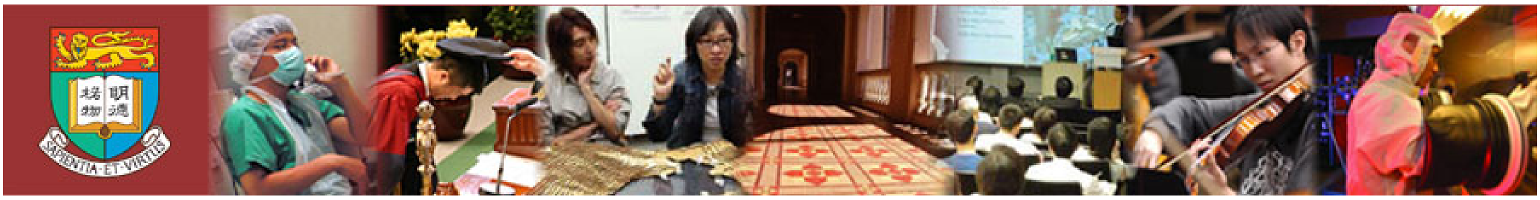

Title	**Screening in Ultrashort (5 nm) Channel MoS2 Transistors: A Full-Band Quantum Transport Study**
Author(s)	**Mishra, V; Smith, S; Liu, L; Zahid, F; Zhu, Y; Guo, H; Salahuddin, S**
Citation	**IEEE Transactions on Electron Devices, 2015, v. 62 n. 8, p. 2457-2463**
Issued Date	**2015**
URL	**http://hdl.handle.net/10722/218807**
Rights	**Creative Commons: Attribution 3.0 Hong Kong License**

Screening in Ultrashort (5 nm) Channel MoS_2 Transistors: A Full-Band Quantum Transport Study

Varun Mishra, Samuel Smith, Lei Liu, Ferdows Zahid, *Member, IEEE*, Yu Zhu, Hong Guo, and Sayeef Salahuddin, *Senior Member, IEEE*

***Abstract*— Full-band ballistic quantum transport calculations were used to study the screening effects in ultrashort-channel few-layer MoS_2 transistors. A large density of states resulted in small screening lengths while inhibiting direct source-to-drain tunneling. Short-channel effects were observed even for the structurally confined 2-D transistors resulting in degraded electrostatic control. Electron confinement effects were also observed in the OFF-state in multilayered devices.**

***Index Terms*— Dichalcogenide, monolayer transistors, MoS_2, nonequilibrium Green's function (NEGF), quantum confinement.**

I. Introduction

Due to a naturally occurring layered structure, large bandgap, and compensated surface, 2-D transition metal dichalcogenides could provide unprecedented gate control [1]–[4] for ultrashort channel length (~5 nm) transistors where conventional semiconductors such as Si and III–V are expected to show a significant short-channel effect [5]. Owing to weak interlayer interactions, Transition Metal Dichalcogenide (TMD) can be exfoliated to fabricate few-layered transistors. Thus, transistors based on TMD materials, especially, MoS_2, have received significant interest in the research community over the last few years [6]–[10]. Models based on effective mass description of the bandstructure show excellent electrostatic properties of MoS_2 transistors with good subthreshold behavior [6] owing to large bandgaps and high effective mass [2], [9], [10]. However, a quantitative understanding of what extent of gate control can actually be achieved, what the determining factors are, and what tradeoffs need to be made requires a more rigorous model of the bandstructure so that the effect of applied voltages on the charge density and, therefore, the current can be appropriately captured. Here, we present a full-band self-consistent quantum transport study of electrostatic screening in 5-nm channel length MoS_2 transistors with doped contacts as a function of number of layers with both single-gate and double-gate geometries. Our results show that for such ultrashort-channel lengths, the following can be observed.

1) The layer closest to the gate can effectively screen out the gate potential due to a large density of states, and as a result, the gate cannot effectively control more than one layer.
2) For a monolayer, a significant short-channel effect can still be observed.
3) Because of 1) and 2), only a double-gate geometry for a monolayer device provides reasonable gate control (subthreshold swing ~84 mV/decade). Surprisingly, these numbers are not better and rather comparable with what could be achieved with a surround-gate Si nanowire of small dimensions (~3-nm diameter) [11].

Manuscript received November 8, 2014; revised June 3, 2015; accepted June 6, 2015. Date of publication June 23, 2015; date of current version July 21, 2015. This work was supported in part by the National Science Foundation through the Early Faculty Development Program Award and in part by the Army Research Office. The review of this paper was arranged by Editor A. Schenk.

V. Mishra, S. Smith, and S. Salahuddin are with the Department of Electrical Engineering and Computer Sciences, University of California at Berkeley, Berkeley, CA 94720 USA (e-mail: vmishra@eecs.berkeley.edu; samuelsmith@berkeley.edu; sayeef@berkeley.edu).

L. Liu and Y. Zhu are with Nanoacademic Technologies Inc., Brossard, QC J4Z 1A7, Canada (e-mail: leo@nanoacademic.ca; eric@nanoacademic.ca).

F. Zahid is with the Department of Physics, The University of Hong Kong, Hong Kong (e-mail: fzahid@hku.hk).

H. Guo is with the Department of Physics, McGill University, Montreal, QC H3A 2T8, Canada (e-mail: guo@physics.mcgill.ca).

Color versions of one or more of the figures in this paper are available online at http://ieeexplore.ieee.org.

Digital Object Identifier 10.1109/TED.2015.2444353

II. Approach

A. Bandstructure

The electronic structure calculations [Fig. 1(a)–(d)] of MoS_2 were performed by fitting orthogonal tight-binding (TB) parameters to density functional theory (DFT) calculations. The parameterization scheme used in this paper follows a similar technique as described in [12], but with improvements that allow for directly including the deviations of bandgaps and effective masses into the minimized cost function [13]–[16]. The obtained TB parameters are listed in Table I, and the corresponding fitting results of bandgaps and effective masses are listed in Tables II and III, respectively. The electronic states near the top of valence bands and the bottom of conduction bands are mainly contributed from Mo d-orbitals and S p-orbitals, mixing with Mo s-orbitals [17]. The energy positions of the states are determined through complicated interactions between those orbitals and many other states in the Hilbert space with higher energies. In order to reproduce the band structure obtained using the first-principle method with high precision, we have also included Mo p-orbitals and S s- and d-orbitals in our TB model, which are used to include the influence of the many other states with higher energies, in an effective way. Therefore, the parameters related to those orbitals may lose their original physical meanings, and should be considered as pure mathematical parameters. The interlayer interactions were included in the bandstructure calculation. This leads to an indirect bandgap for few-layered

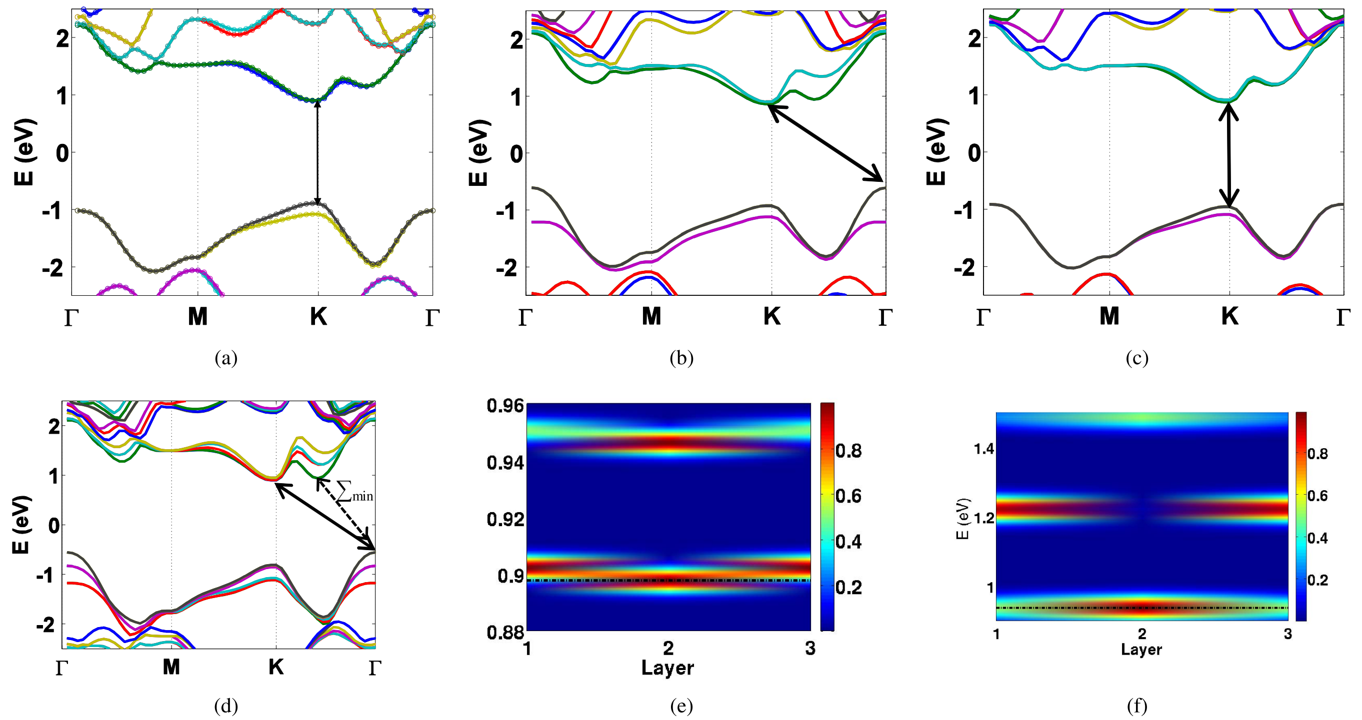

Fig. 1. Electronic structure computed from TB models along high symmetry lines for (a) monolayer MoS_2 (electronic structure from DFT calculations marked with circles), for bilayer MoS_2 calculated using TB models with the interaction between the two layers turned (b) ON and (c) OFF, and for (d) three-layer MoS_2. The bandgap of monolayer MoS_2 is 1.8 eV with the offset between the K (conduction band minimum) and Σ_{min} (minimum energy point along the $K - \Gamma$ direction) valleys equal to 0.2503 eV. The valence band maximum for monolayer MoS_2 shifts from the K point to the Γ point when the interaction is turned ON resulting in an indirect bandgap. The bandgap of bilayer MoS_2 is equal to 1.48 eV, while that of three-layer MoS_2 is 1.46 eV. The conduction band minimum shifts from K to Σ_{min} as the number of layers is increased from three. The layer-wise projected density of states for the eigenstates at the bottom of conduction band at (e) K and (f) Σ_{min} points for three-layer MoS_2 show a higher confinement of electrons in the middle layer. The bottom of the conduction band is shown by the dotted black line. A lower temperature was used at the K point as opposed to room temperature used at the Σ_{min} point to show the confinement effects at the K point as the eigenstates are closer to each other. The effect is thus less significant at the K point compared with the Σ_{min} point.

MoS_2 as shown in Fig. 1(a) and (b). The bandgaps from the TB parameters were calculated to be 1.8, 1.48, and 1.46 eV for monolayer, bilayer, and three-layer MoS_2, respectively. The bandstructure matches well with previous theoretical and experimental results [18]. Monolayer MoS_2 has a direct bandgap at the K point. The valence band maximum shifts to the Γ point for few-layered devices, while it shifts back from the Γ point to K point if the interlayer interactions are removed, showing their significance, especially in p-type transport. The conduction band minimum also shifts from the K point to Σ_{min} (local minimum along $K - \Gamma$) point as the number of layers is increased from three. In this paper, we will investigate only the electronic properties of one- to three-layered transistors.

One important observation for multilayer (e.g., the three-layer) structures is the fact that increased surface energy leads to a higher projected density of eigenstates in the inner layer [Fig. 1(e) and (f)]. The layer-wise density was calculated by normalizing the eigenvector corresponding to a certain energy and momentum and summing over the probability of all the orbitals belonging to a layer. The probability density of eigenstates at the bottom of the conduction band at both the K and Σ_{min} points shows a considerable confinement of electrons to the inner layer, thus resulting in higher charge densities in those layers. There is reasonably large density of states in the surface layers 100 meV above the band minimum at the Σ_{min} point while it is significant 20 meV from the minimum at the K point. Thus, the effect will be more significant for multilayered devices, as Σ_{min} becomes the conduction band minimum. A higher current could be expected in the middle layer in the OFF-state for three-layered transistors, if the electric field can penetrate through the top most layer.

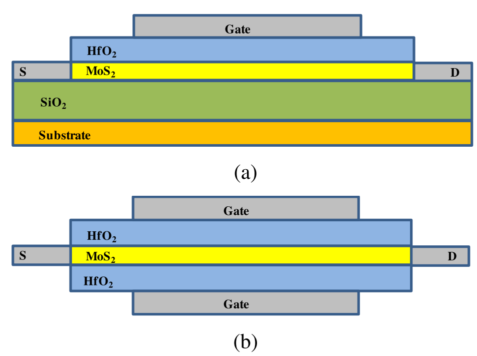

Fig. 2. Schematic of the simulated layered MoS_2 transistors with (a) single gate and (b) double gates. The gate length is 5 nm. The number of layers of TMDs is varied from 1 to 3, resulting in a body thickness in the range of 0.6–1.8 nm. The source and drain contacts are ohmic (no Schottky barrier). EOT is 0.5 nm.

B. Device Simulation

The schematic of the simulated device structures along with the device parameters is shown in Fig. 2. We use both

TABLE I

TB PARAMETERS FOR MoS_2 USING ORTHOGONAL MODEL WITH sp^3d^5 ORBITALS, NEAREST-NEIGHBOR INTERACTIONS, AND SPIN-ORBIT COUPLING, IN THE UNIT OF ELECTRONVOLTS

	Single Layer	Double Layer	Bulk
On-site energy			
s(S)	17.9023	17.4692	17.2848
p(S)	-2.4009	-2.6415	-2.2950
d(S)	75.2885	75.1980	74.6303
s(Mo)	9.9447	9.7433	10.1452
p(Mo)	36.6985	37.4747	36.2812
d(Mo)	4.1225	4.3256	4.2039
Spin-orbit splitting λ_{SO}			
p(S)	0.05388	0.2446	0.3126
p(Mo)	0.9235	0.8246	1.5907
Slater-Koster energy integral (intra-layer)			
$s(S)s(S)\sigma$	-0.8590	-0.5104	-0.4557
$s(S)p(S)\sigma$	-0.2142	-0.1193	-0.2661
$p(S)p(S)\sigma$	0.8715	0.9152	0.9406
$p(S)p(S)\pi$	-0.2449	-0.2604	-0.3175
$s(S)d(S)\sigma$	3.1818	3.3973	3.6853
$p(S)d(S)\sigma$	0.1138	-0.4924	0.2515
$p(S)d(S)\pi$	-0.4476	0.2920	-0.3709
$d(S)d(S)\sigma$	3.7203	-2.7489	3.6162
$d(S)d(S)\pi$	-2.5901	-2.7489	-1.3972
$d(S)d(S)\delta$	-1.1719	-1.0508	-1.3690
$s(Mo)s(Mo)\sigma$	-1.5166	-1.4157	-1.4603
$s(Mo)p(Mo)\sigma$	0.4991	0.5353	0.1376
$p(Mo)p(Mo)\sigma$	-3.8198	-4.4557	-5.3723
$p(Mo)p(Mo)\pi$	4.5562	4.6003	4.3870
$s(Mo)d(Mo)\sigma$	0.007971	0.06601	0.3100
$p(Mo)d(Mo)\sigma$	1.3306	1.0464	1.3263
$p(Mo)d(Mo)\pi$	0.95906	-0.3587	-0.3780
$d(Mo)d(Mo)\sigma$	0.95906	1.0819	0.9623
$d(Mo)d(Mo)\pi$	-0.452	-0.3991	-0.4319
$d(Mo)d(Mo)\delta$	0.5143	0.4971	0.4623
$s(S)s(Mo)\sigma$	-0.1246	0.4253	0.1484
$s(S)p(Mo)\sigma$	3.9553	4.3327	3.7256
$p(S)p(Mo)\sigma$	1.2385	0.9410	1.1730
$p(S)p(Mo)\pi$	-0.2589	-0.3840	-0.4290
$s(S)d(Mo)\sigma$	1.6798	1.2016	1.6079
$p(S)d(Mo)\sigma$	-2.8710	-2.7683	-2.9008
$p(S)d(Mo)\pi$	0.8901	0.8137	0.9168
$d(S)d(Mo)\sigma$	4.8937	5.7088	5.0221
$d(S)d(Mo)\pi$	-9.3391	-9.3064	-9.2758
$d(S)d(Mo)\delta$	1.2478	1.1624	1.6762
$s(S)d(Mo)\sigma$	1.6798	1.2016	1.6079
$s(Mo)p(S)\sigma$	1.1862	1.0713	1.0930
$s(Mo)d(S)\sigma$	10.4024	9.5661	9.9100
$p(Mo)d(S)\sigma$	16.3744	16.4443	16.2916
$p(Mo)d(S)\pi$	-16.6761	-16.7952	-16.4873
Slater-Koster energy integral (inter-layer)			
$s(S)s(S)\sigma$		0.3665	-0.1649
$s(S)p(S)\sigma$		-0.7006	-0.03491
$p(S)p(S)\sigma$		0.4188	0.3206
$p(S)p(S)\pi$		0.07841	0.06415
$s(S)d(S)\sigma$		-0.09494	0.5781
$p(S)d(S)\sigma$		0.8274	1.0903
$p(S)d(S)\pi$		-0.6468	-0.6043
$d(S)d(S)\sigma$		-0.1055	-0.4620
$d(S)d(S)\pi$		-1.2847	-0.7753
$d(S)d(S)\delta$		-0.5428	-0.9156

single-gated (SG) and double-gated (DG) devices in this paper. The oxide thickness for each gate-stack has an effective oxide thickness of 0.5 nm. Highly doped [19] contacts, with a doping concentration of 3×10^{13} cm^{-2}, are used in the source and drain regions. A small underlap is used to reduce fringe capacitances from the source and drain regions as well as to inhibit direct source–drain tunneling [20]. The workfunction difference between the gate and channel is assumed to be zero. The width of each device was assumed to be large enough so that a mode space summation could be used along that direction, while a real space representation was used along the direction of transport [21]. The TB parameters fitted from

TABLE II

BANDGAP ENERGIES OBTAINED BY DFT-HSE [12] AND OUR TB MODEL. THE FIFTH COLUMN IS THE DEVIATION BETWEEN THE HEYD-SCUSERIA-ERNZERHOF (HSE) AND THE TB VALUES. ALL THE ENERGIES ARE IN THE UNIT OF ELECTRONVOLTS. SUBSCRIPTS v AND c STAND FOR VALENCE BAND AND CONDUCTION BAND, RESPECTIVELY. THE SPLITTING OF THE VALENCE BAND MAXIMUM AT K POINT IS GIVEN BY K_{v1} (TOP) AND K_{v2} (BOTTOM), WHEREAS Σ IS THE MIDPOINT OF THE LINE JOINING THE Γ AND THE K POINTS

Structure	Transitions	Band-gap energies (eV)		
		HSE (target)	TB (fitted)	Deviation%
Monolayer	K_{v1} to K_c	1.7857	1.7857	0.00
	K_{v2} to K_c	1.9742	1.9742	0.00
	Γ_v to K_c	1.9457	1.9123	-1.72
	Γ_v to Σc	2.2252	2.1613	-2.87
Bilayer	Γ_v to K_c	1.4801	1.4749	-0.36
	Γ_v to Σ_c	1.6178	1.5532	-3.99
	K_{v1} to K_c	1.7787	1.7894	0.60
	K_{v2} to K_c	1.9802	1.9829	0.14
Bulk	Γ_v to Σ_c	1.3280	1.3280	0.00
	Γ_v to K_c	1.3661	1.3543	-0.86
	K_{v1} to K_c	1.7751	1.6755	-5.61
	K_{v2} to K_c	1.9985	2.0411	2.13

TABLE III

VALUES OF EFFECTIVE MASSES AT VARIOUS BAND EDGES IN THE UNIT OF FREE ELECTRON MASS (m_0) CALCULATED USING THE HSE METHOD [12] AND OUR TB MODEL. THE SUBSCRIPTS l AND t REFER TO THE MASSES CALCULATED AT THE POINT ALONG THE LONGITUDINAL AND THE TRANSVERSE DIRECTIONS OF THE LINE CONNECTING THE Γ POINT AND THAT POINT, RESPECTIVELY

		Electron mass (m_0)			Hole mass (m_0)		
Structure	Point	HSE (target)	TB (fitted)	Deviation (%)	HSE (target)	TB (fitted)	Deviation (%)
Mono-layer	K_l	0.4065	0.4072	0.16	0.4852	0.4855	0.06
	K_t	0.4035	0.4031	-0.10	0.4804	0.4802	-0.05
Bilayer	Γ				1.0387	1.0387	0.00
	K_l	0.4302	0.4275	-0.63	0.4851	0.4853	0.03
	K_t	0.4227	0.4260	0.79	0.4810	0.4853	-0.21
Bulk	Γ				0.7849	0.7849	0.00
	Σ_l	0.5737	0.5737	0.00			
	Σ_t	0.8186	0.8186	0.00			

the DFT calculations were used to formulate the full-band Hamiltonian for each of the considered devices. The charge was calculated within the nonequilibrium Green's function (NEGF) formalism [22], [23]. The calculated charge was then used by a finite-difference Poisson solver with appropriate boundary conditions to calculate the potential corresponding to the charge [24]. Dirichlet boundary conditions are used at the gate contacts, while Neumann boundary conditions are assumed at the electrostatic domain boundary for doped contacts so that the electric potential profile floats to ensure charge neutrality at the boundaries. This was then used by the transport solver to achieve a self-consistent solution for each bias point. The transmission $T(E)$ as a function of energy was then calculated using the converged potential profile along the channel, while summing over all the transverse modes. Scattering effects could be considered to be minimal at these channel lengths. The valence band could be ignored in most of the calculations, because of the large bandgap of MoS_2 and hence a lack of band-to-band tunneling. The total current was

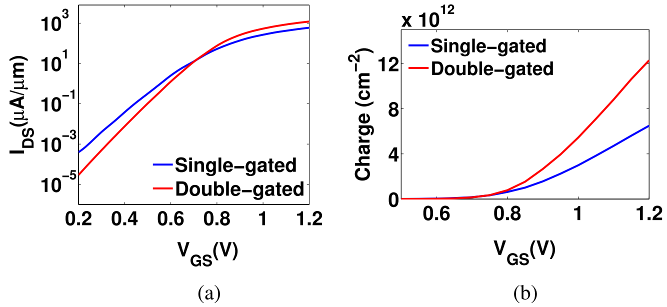

Fig. 3. (a) I_{DS}–V_{GS} characteristics and (b) charge density at the top of the barrier for SG and DG monolayer MoS_2 transistors at $V_{DS} = 0.05$ V. The DG transistor has significantly better electrostatic control with better subthreshold swing and higher ON-currents. The charge density is about two times higher for DG transistors.

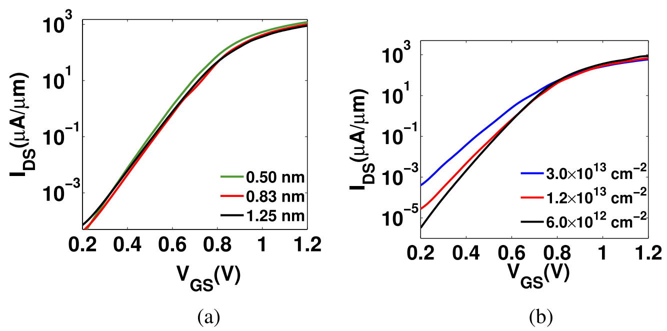

Fig. 4. I_{DS}–V_{GS} characteristics of (a) DG monolayer MoS_2 transistors with a top oxide thickness of 0.5 nm and varying bottom oxide thickness and (b) SG monolayer transistors with varying source–drain doping concentration at $V_{DS} = 0.05$ V. The gate control goes down with increased oxide thickness. The drain control increases with higher doping concentration leading to worse electrostatic control.

then calculated by summing the transmission over the energy grid by weighting it with the difference in Fermi distribution at the source and drain

$$I = \sum_E dE\ T(E)(f(E-\mu_S) - f(E-\mu_D)) \tag{1}$$

where $f(E)$ is the Fermi–Dirac distribution, while μ_S and μ_D are the chemical potentials at the source and drain, respectively.

III. Results and Discussion

The I_{DS}–V_{GS} characteristics for SG and DG MoS_2 for low drain voltage ($V_{DS} = 0.05$ V) are shown in Fig. 3. The DG device (SS $\sim$ 84 mV/decade) shows better performance than the SG device (SS $\sim$ 102 mV/decade) even in the case of a monolayer demonstrating significant short-channel effects. The charge accumulated at the top of the barrier is almost twice for the DG device compared with the SG device showing a considerably higher gate control. There is a need of further scaled gate oxides at these gate lengths to achieve reasonable performance characteristics. Fig. 4(a) compares I_{DS}–V_{GS} characteristics for DG monolayer devices with a fixed top oxide thickness of 0.5 nm and varying bottom oxide thickness. The subthreshold behavior degrades with increased bottom oxide thickness and tends to resemble the SG device.

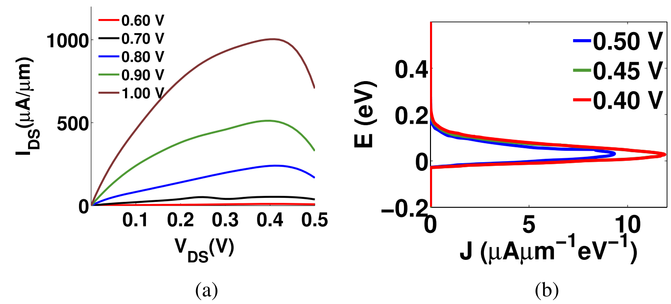

Fig. 5. (a) I_{DS}–V_{DS} characteristics of monolayer MoS_2 transistors. (b) Current spectrum as a function of energy. Negative differential resistance can be observed in the transistors at high drain voltages due to limited bandwidth. The effect is confirmed in the current spectrum as transmission reduces beyond a drain voltage of 0.45 V.

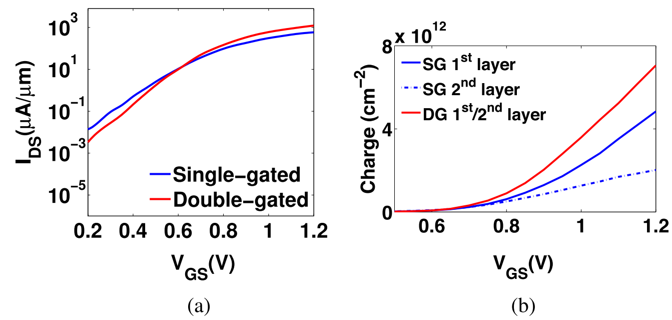

Fig. 6. (a) I_{DS}–V_{GS} characteristics and (b) charge density at the top of the barrier for SG and DG (each layer) bilayer MoS_2 transistors at $V_{DS} = 0.05$ V. The DG transistor shows better performance owing to greater gate control. The charge on the second layer is significantly lower than on the first layer showing a small effective screening length.

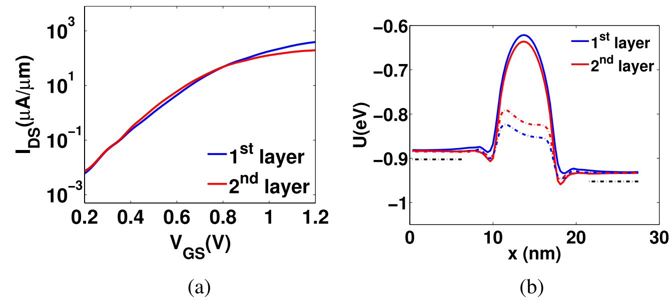

Fig. 7. (a) Layer-wise current for single-gate bilayer MoS_2 at $V_{DS} = 0.05$ V. (b) Potential profile along the channel at $V_{GS} = 0.40$ V (solid lines) and $V_{GS} = 1.10$ V (dashed lines). The first layer has higher current for higher gate voltages while showing marginally lower OFF-current. The potential barrier is lower for the top layer at high gate voltages resulting in higher current.

The I_{DS}–V_{GS} characteristics for monolayer SG MoS_2 shown in Fig. 4(b) demonstrate the increased drain control as the contact doping is increased leading to degraded subthreshold behavior. The I_{DS}–V_{DS} characteristics are shown in Fig. 5(a) for SG monolayer MoS_2 at different gate biases. Negative differential resistance can be observed for high drain voltages (V_{DS} greater than 0.45 V) because of limited bandwidth of the first few bands. The current spectrum as a function of energy as shown in Fig. 5(b) for $V_{DS} = 0.40$ and 0.45 V lies on top of each other, while that of $V_{DS} = 0.50$ V is lower. This effect has been observed before and is a manifestation

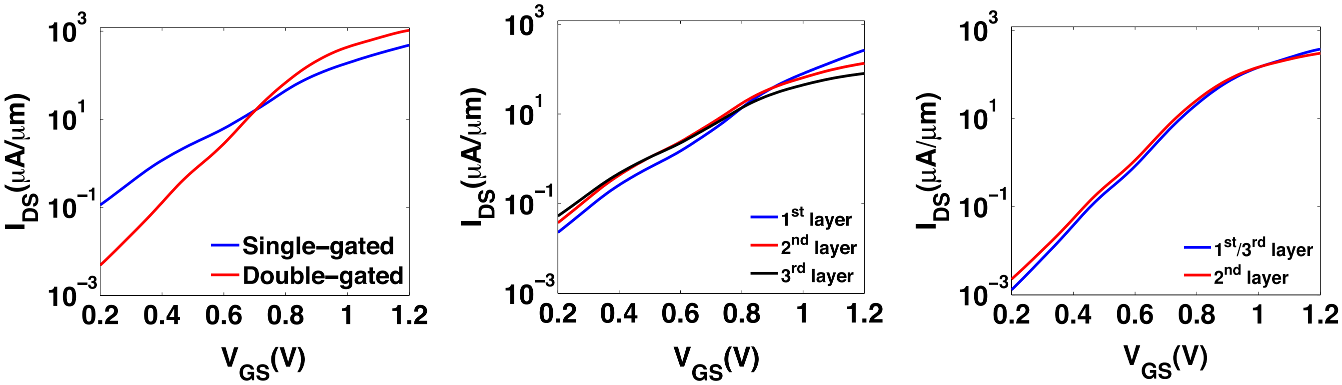

(a) (b) (c)

Fig. 8. (a) I_{DS}–V_{GS} characteristics of SG and DG three-layer MoS_2 transistors at $V_{DS} = 0.05$ V. Layer-wise current for (b) single-gate and (c) double-gate three-layer transistor. The DG transistor shows better performance with higher ON-currents and lower OFF-currents. The third layer provides the maximum current in the OFF-state due to lower gate control, while it has the lowest current in the ON-state due to screening from the top layer single-gate devices. The middle layer carries maximum current in the OFF-state owing to higher confinement of electrons, while it is screened in the ON-state for double-gate transistors.

of ballistic transport, which may not be observable in experiments because of electron–phonon scattering [25], [26]. Electron–phonon coupling introduces transmission channels among different transverse modes, thus eliminating the gap in current transmission.

Going on to bilayer, Fig. 6(a) shows a comparison of I_{DS}–V_{GS} characteristics of SG versus DG bilayer MoS_2 at low drain voltage. Bilayer MoS_2 shows much weaker gate control compared with monolayer MoS_2; SS $\sim$ 109 and 140 mV/decade for DG and SG, respectively. The charge density at the top of the barrier in Fig. 6(b) shows the screening of the second layer from the gate by the top layer in the ON-state. The current contribution from the second layer is therefore significantly less than that of the top layer. The subthreshold swing goes down to 90 mV/decade for a doping concentration of 6×10^{12} cm^{-2}. Fig. 7 shows the loss in gate control of the bottom layer in both the ON and OFF states. The barrier to current flow is higher in the OFF-state for the top layer resulting in marginally lower current, while it is significantly lower in the ON-state, thus screening the bottom layer from the gate. These results underline the significant screening effect by charge accumulated at the layer closest to the gate and therefore poor gate control of any additional layers. Because of these small screening lengths, the DG bilayer behaves like two SG monolayer transistors resulting in similar transfer characteristics to the same.

To test the consistency of these results, we have further investigated a three-layer device. The higher gate control of DG compared with SG three-layer transistors can be observed in Fig. 8(a), with lower OFF- and ON-currents in the DG device. Fig. 8(b) shows layer-wise currents for the SG three-layer device, where the bottom layer contributes the highest current in the OFF-state, while the top layer conducts most of the current in the ON-state, showing that the change in thermal barrier to current flow is the highest for the top layer. The DG three-layer device shows similar characteristics with the middle layer carrying the lowest current in the ON-state, while some confinement effects can be observed in the OFF-state [Fig. 8(c)]. The middle layer carries more current

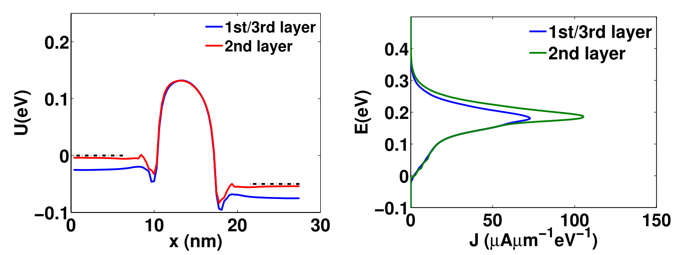

(a) (b)

Fig. 9. (a) Electric potential profile along the channel for double-gate three-layer devices. (b) Current density as a function of energy at $V_{GS} = 0.75$ V (OFF-state). The middle layer carries greater current compared with the surface layer due to higher confinement of eigenstates. The conduction band is further below the Fermi level for the surface layers owing to the same reason.

than the surface layers in the OFF-state, i.e., for $V_{GS} = 0.8$ V. This effect, which is a consequence of higher Density of States (DOS) near the band edge in the middle layer [Fig. 1(e) and (f)], is further illustrated in Fig. 9. Fig. 9(a) shows the potential profile along the channel for the DG three-layer device at $V_{GS} = 0.75$ V. The conduction band is further below the Fermi level for the surface layers compared with the middle layer, because of higher concentration of electrons toward the center of the channel. The barrier height of the electrons from the Fermi level is the same for all the layers at this bias point as screening effects are not significant. The current density as a function of energy

$$J(E) = T(E)(f(E - \mu_S) - f(E - \mu_D)) \tag{2}$$

is shown in Fig. 9(b) at the same bias point. As expected, higher current is drawn from the middle layer because of increased surface energy for the outer layers. Both the surface layers have similar characteristics because of symmetry in the simulated device.

The I_{DS}–V_{GS} characteristics at $V_{DS} = 0.50$ V for all devices considered are shown in Fig. 10(a), while the ON-current for the corresponding ON/OFF is shown in Fig. 10(b). The transfer characteristics follow similar trends as the previous results

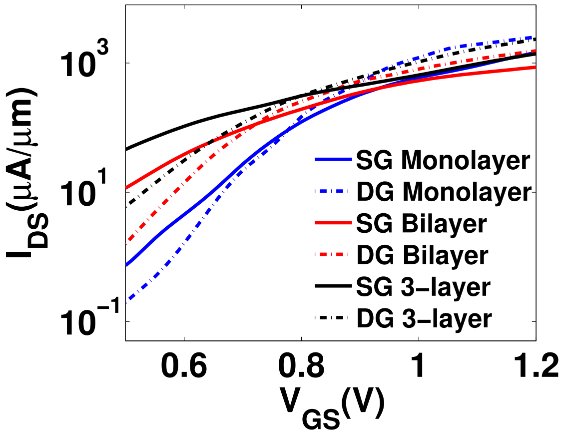

(a)

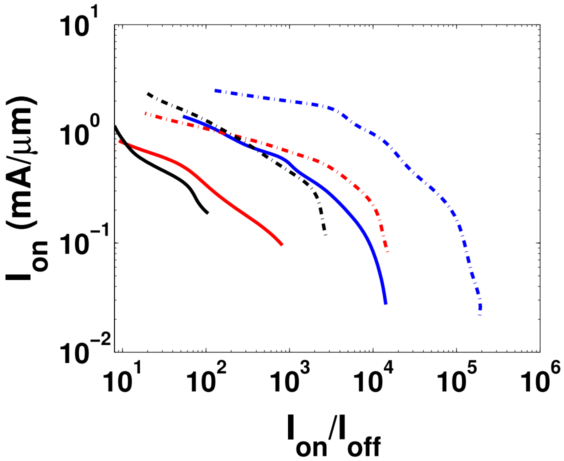

(b)

Fig. 10. (a) I_{DS}–V_{GS} characteristics of single- and double-gate monolayer, bilayer, and three-layer MoS_2 transistors at $V_{DS} = 0.50$ V. (b) ON-current for the above transistors as a function of ON/OFF ratios at $V_{DD} = 0.50$ V. The DG monolayer transistor shows the best ON-currents for a given ON/OFF, achieving the highest ON-current and lowest OFF-current. The trends for the three-layer devices move toward worse ON/OFF ratios.

with DG monolayer showing the best ON- and OFF-currents. The SG monolayer device shows a Drain Induced Barrier Lowering (DIBL) of 70 mV/V, while the bilayer device shows a DIBL of 300 mV/V, showing significant drain control at these scales. The DIBL for the DG monolayer device is 30 mV/V showing that better performance characteristics could be achieved through Effective Oxide Thickness (EOT) scaling. The ON/OFF ratios shown in Fig. 10(b) correspond to a supply voltage of 0.50 V, while the bias window for gate voltage is moved along the transfer characteristics. The above could be achieved in practice by engineering the workfunction of the gate metal [27]. None of the SG devices were able to achieve an ON/OFF of 10^5, the minimum ratio needed to be considered as a viable alternative for low operating power transistors. Only DG monolayer device achieved an ON/OFF of 10^5, but at an ON-current of 90 μA/μm. The trends for SG monolayer transistor are similar to those of the DG bilayer transistors with the bilayer device having higher current levels. The three-layer devices show worse ON/OFF ratios because of increased screening effects.

IV. Conclusion

To summarize, layered MoS_2 transistors with doped contacts and 5-nm channel length were studied using a full-band self-consistent quantum transport model within the ballistic NEGF formalism. One of the interesting observations from this full-band study is the fact that in a multilayer structure, the middle layers give the lowest energy states and would therefore fill up first. This effect is evident in our calculations for small charge levels when the gate electric field can still penetrate through the top layers. As for the current–voltage behavior, the ballistic approximation is relevant in the view that the gate length is only 5 nm. In addition, together with a doped contact, the ballistic approximation provides the best case scenario for these devices. It is observed that the ballistic ON-current for these devices for a V_{DD} swing of 0.5 V is not competitive with what can be otherwise obtained from Si, III-V, or carbon nanotube devices at this channel length. This is not surprising because the injection velocity for MoS_2 is small due to its large effective mass. It also found that it is not possible to boost the ON-current up by increasing the number of layers at this channel length because the gate electric field (for ∼0.5-nm EOT) is almost completely screened out by the layer nearest to the gate. As a result, layers underneath cannot be effectively controlled by the gate, leading to significant reduction in subtheshold swing. In fact, even for a single monolayer, the short channel effect is prominent and only a double-gate geometry can provide a reasonable subthreshold swing (∼84 mV/decade). Surprisingly, this is comparable with (and not better than) what has been predicted to be achievable with surround-gate small-diameter (∼3 nm) Si nanowire transistors [11]. On the other hand, a double-gate geometry for a monolayer structure may prove to be very challenging to fabricate. However, one particular aspect stands out: MoS_2 transistors could provide a 10^5 ON/OFF ratio even at 5-nm channel length, albeit at a small ON-current level, which is not possible at all in Si or III-V due to much stronger direct source-to-drain tunneling. This indicates potential use in very low power applications where performance is not a critical need.

References

[1] K. F. Mak, C. Lee, J. Hone, J. Shan, and T. F. Heinz, "Atomically thin MoS_2: A new direct-gap semiconductor," *Phys. Rev. Lett.*, vol. 105, no. 13, p. 136805, 2010.

[2] Y. Yoon, K. Ganapathi, and S. Salahuddin, "How good can monolayer MoS_2 transistors be?" *Nano Lett.*, vol. 11, no. 9, pp. 3768–3773, 2011.

[3] J. A. Wilson and A. D. Yoffe, "The transition metal dichalcogenides discussion and interpretation of the observed optical, electrical and structural properties," *Adv. Phys.*, vol. 18, no. 73, pp. 193–335, 1969.

[4] Q. H. Wang, K. Kalantar-Zadeh, A. Kis, J. N. Coleman, and M. S. Strano, "Electronics and optoelectronics of two-dimensional transition metal dichalcogenides," *Nature Nanotechnol.*, vol. 7, no. 11, pp. 699–712, 2012.

[5] V. Mishra, S. Smith, K. Ganapathi, and S. Salahuddin, "Dependence of intrinsic performance of transition metal dichalcogenide transistors on materials and number of layers at the 5 nm channel-length limit," in *IEDM Tech. Dig.*, Dec. 2013, pp. 5.6.1–5.6.4.

[6] A. Splendiani *et al.*, "Emerging photoluminescence in monolayer MoS_2," *Nano Lett.*, vol. 10, no. 4, pp. 1271–1275, 2010.

[7] W. Ho, J. C. Yu, J. Lin, J. Yu, and P. Li, "Preparation and photocatalytic behavior of MoS_2 and WS_2 nanocluster sensitized TiO_2," *Langmuir*, vol. 20, no. 14, pp. 5865–5869, 2004.

[8] B. Radisavljevic, A. Radenovic, J. Brivio, V. Giacometti, and A. Kis, "Single-layer MoS_2 transistors," *Nature Nanotechnol.*, vol. 6, no. 3, pp. 147–150, 2011.
[9] K. Alam and R. K. Lake, "Monolayer MoS_2 transistors beyond the technology road map," *IEEE Trans. Electron Devices*, vol. 59, no. 12, pp. 3250–3254, Dec. 2012.
[10] L. Liu, Y. Lu, and J. Guo, "On monolayer MoS_2 field-effect transistors at the scaling limit," *IEEE Trans. Electron Devices*, vol. 60, no. 12, pp. 4133–4139, Dec. 2013.
[11] M. Luisier, M. Lundstrom, D. A. Antoniadis, and J. Bokor, "Ultimate device scaling: Intrinsic performance comparisons of carbon-based, InGaAs, and Si field-effect transistors for 5 nm gate length," in *Proc. IEEE Int. Electron Devices Meeting (IEDM)*, Dec. 2011, pp. 11.2.1–11.2.4.
[12] F. Zahid, L. Liu, Y. Zhu, J. Wang, and H. Guo. (2013). "A generic tight-binding model for monolayer, bilayer and bulk MoS_2." [Online]. Available: http://arxiv.org/abs/1304.0074
[13] Nanoacademic Technologies. (2013). *Nanoskif*. [Online]. Available: http://www.nanoacademic.com/
[14] J. C. Slater and G. F. Koster, "Simplified LCAO method for the periodic potential problem," *Phys. Rev.*, vol. 94, no. 6, pp. 1498–1524, 1954.
[15] D. J. Chadi, "Spin-orbit splitting in crystalline and compositionally disordered semiconductors," *Phys. Rev. B, Condens. Matter*, vol. 16, no. 2, pp. 790–796, 1977.
[16] T. Cheiwchanchamnangij and W. R. L. Lambrecht, "Quasiparticle band structure calculation of monolayer, bilayer, and bulk MoS_2," *Phys. Rev. B, Condens. Matter*, vol. 85, no. 20, p. 205302, 2012.
[17] L. F. Mattheiss, "Band structures of transition-metal-dichalcogenide layer compounds," *Phys. Rev. B*, vol. 8, no. 8, pp. 3719–3740, Oct. 1973. [Online]. Available: http://link.aps.org/doi/10.1103/PhysRevB.8.3719
[18] J. K. Ellis, M. J. Lucero, and G. E. Scuseria, "The indirect to direct band gap transition in multilayered MoS_2 as predicted by screened hybrid density functional theory," *Appl. Phys. Lett.*, vol. 99, no. 26, p. 261908, 2011.
[19] H. Fang *et al.*, "Degenerate n-doping of few-layer transition metal dichalcogenides by potassium," *Nano Lett.*, vol. 13, no. 5, pp. 1991–1995, 2013.
[20] A. Bansal, B. C. Paul, and K. Roy, "Impact of gate underlap on gate capacitance and gate tunneling current in 16 nm DGMOS devices," in *Proc. IEEE Int. SOI Conf.*, Oct. 2004, pp. 94–95.
[21] R. Venugopal, Z. Ren, S. Datta, M. S. Lundstrom, and D. Jovanovic, "Simulating quantum transport in nanoscale transistors: Real versus mode-space approaches," *J. Appl. Phys.*, vol. 92, no. 7, pp. 3730–3739, 2002.
[22] S. Datta, *Quantum Transport: Atom to Transistor*. Cambridge, U.K.: Cambridge Univ. Press, 2005.
[23] M. P. Anantram, M. S. Lundstrom, and D. E. Nikonov, "Modeling of nanoscale devices," *Proc. IEEE*, vol. 96, no. 9, pp. 1511–1550, Sep. 2008.
[24] Z. Ren, "Nanoscale MOSFETs: Physics, simulation and design," Ph.D. dissertation, Dept. Elect. Comput. Eng., Purdue Univ., West Lafayette, IN, USA, 2001.
[25] A. Szabo, R. Rhyner, and M. Luisier, "Ab-initio simulations of MoS_2 transistors: From mobility calculation to device performance evaluation," in *Proc. IEEE Int. Electron Devices Meeting (IEDM)*, Dec. 2014, pp. 30.4.1–30.4.4.
[26] J. Chang, L. F. Register, and S. K. Banerjee, "Atomistic full-band simulations of monolayer MoS_2 transistors," *Appl. Phys. Lett.*, vol. 103, no. 22, p. 223509, 2013. [Online]. Available: http://scitation.aip.org/content/aip/journal/apl/103/22/10.1063/1.4837455
[27] Y. Taur and T. H. Ning, *Fundamentals of Modern VLSI Devices*, vol. 2. Cambridge, U.K.: Cambridge Univ. Press, 1998.

Varun Mishra is currently pursuing the Ph.D. degree with the Department of Electrical Engineering and Computer Sciences, University of California at Berkeley, Berkeley, CA, USA.

His current research interests include modeling and simulation of nanoscale devices with a focus on layered materials.

Samuel Smith is currently pursuing the Ph.D. degree with the Department of Electrical Engineering and Computer Sciences, University of California at Berkeley, Berkeley, CA, USA.

His current research interests include computational modeling of novel device physics.

Lei Liu received the Ph.D. degree in theoretical and computational atomic and molecular physics from the Institute of Physics, Chinese Academy of Sciences, Beijing, China, in 1991.

He is currently a Senior Scientist with Nanoacademic Technologies Inc., Brossard, QC, Canada. His current research interests include computational materials, electronics, chemistry, and physics.

Ferdows Zahid (M'09) received the Ph.D. degree from Purdue University, West Lafayette, IN, USA.

He has been with the Department of Physics, The University of Hong Kong, Hong Kong, since 2010.

Yu Zhu received the Ph.D. degree in theoretical physics from the Department of Physics, Peking University, Beijing, China, in 2003.

He is currently a Senior Scientist with NanoAcademic Technologies Inc., Brossard, QC, Canada.

Hong Guo received the Ph.D. degree in theoretical condensed matter physics from the University of Pittsburgh, Pittsburgh, PA, USA, in 1987.

He is currently a James McGill Professor of Physics with McGill University, Montréal, QC, Canada

Sayeef Salahuddin (SM'14) is currently an Associate Professor with the Department of Electrical Engineering and Computer Sciences, University of California at Berkeley, Berkeley, CA, USA.

His current research interests include the emerging device technologies for energy efficient computing.